Waveform Proportionality and Taylor's Law Induced by Synchronization of Periodic and Chaotic Oscillators

Yuzuru Mitsui* and Hiroshi Kori
Department of Complexity Science and Engineering, The University of Tokyo, Kashiwa, Chiba 277-8561, Japan

(Received 27 November 2023; accepted 19 February 2025; published 25 April 2025)

Taylor's law (TL), the scaling relationship between mean and variance, has been observed in various fields. However, the underlying reasons for the widespread occurrence of TL, the frequent appearance of the TL exponent value close to 2, and the relationship between temporal and spatial TLs are not fully understood. Here, using coupled oscillator models, we analytically and numerically demonstrate that synchronization can induce TL. In particular, we show that strong synchronization leads to waveform proportionality, resulting in temporal and spatial TLs with an exponent 2. Our results can help infer the existence of synchronization solely from the correlation between mean and variance.

DOI: 10.1103/PhysRevLett.134.167202

Introduction—Taylor's law [1,2] (TL), a power-law relationship between mean and variance: $\log(\text{variance}) = \log\alpha + \beta \times \log(\text{mean})$, has been observed in various fields, such as population ecology [2], biophysics [3], and complex networks [4–6], among others [7,8]. TL is also known as fluctuation scaling in physics [7]. Especially, when $\beta > 1$, this power-law relationship is sometimes called giant number fluctuations, which have been investigated experimentally [9,10] and theoretically [11–13], and have garnered considerable attention in the field of active matter [14–16]. TL has been extensively analyzed via theoretical studies [3,4,6,17–35], and it is usually classified into two types, i.e., temporal TL and spatial TL. For temporal TL, the means and variances are computed from data recorded at multiple time points at a specific location, whereas for spatial TL, the means and variances are computed from data recorded at multiple locations at a specified time point.

Various studies have been conducted to clarify the mechanisms of TL. Although theories show that β can take any real value [17–19], $\beta \simeq 2$ has been often observed in ecosystems for both temporal and spatial TLs [20,21,36]. Cohen and Xu showed that when multiple independent random variables follow the same distribution, a correlation appears between mean and variance upon random sampling if the distribution is skewed [22]. While their results shed light on the ubiquity of TL, the reason for frequently observing $\beta \simeq 2$ in ecosystems remains unclear because β can take arbitrary values depending on the shape of the distribution. By applying large deviations theory and finite-sample arguments, Giometto *et al.* showed that, depending on the sampling method, $\beta \simeq 2$ may be frequently observed in spatial TL [23]. Reuman *et al.* showed that correlations between random variables affect β of spatial TL [24]. In particular, spatial TL with $\beta = 2$ is observed when a proportional relationship exists between time series [24]. As a mechanism for the emergence of TL with $\beta \simeq 2$, the correlation between time series is considered crucial, and synchronization is strongly implicated as the mechanism that generates such correlations. Moreover, studies employing numerical simulations of dynamical systems have shown that synchronization affects both temporal and spatial TL exponents [21,25,26]. Notably, when the degree of correlation between time series increases, the exponents of temporal and spatial TLs approach 2 [20,27,37].

In this study, we showed that in a broad class of dynamical system models, including ecological models, synchronization generates a special correlation between time series, which we call waveform proportionality, resulting in temporal and spatial TLs with $\beta = 2$.

Model and results—First, we define TL for a given time-series set $x_i(t)$ $(i = 1, \ldots, N)$. For temporal TL, we compute the mean and variance of each site i as $\mathrm{E}[x_i(t)]_t = \langle x_i(t)\rangle_t$ and $\mathrm{V}[x_i(t)]_t = \langle (x_i(t) - \mathrm{E}[x_i(t)]_t)^2\rangle_t$, respectively, where $\langle\cdot\rangle_t$ denotes the long-time average or average over 1 cycle when $x_i(t)$ is periodic. A linear fitting to N data points of $(\log \mathrm{E}[x_i(t)]_t, \log \mathrm{V}[x_i(t)]_t)$ yields slope β_t and intercept $\log\alpha_\mathrm{t}$. For spatial TL, the mean and variance at time t are expressed by $\mathrm{E}[x_i(t)]_i = \langle x_i(t)\rangle_i$ and $\mathrm{V}[x_i(t)]_i = \langle (x_i(t) - \mathrm{E}[x_i(t)]_i)^2\rangle_i$, respectively, where $\langle\cdot\rangle_i$ denotes the average over site i. A linear fitting to M data points of $(\log \mathrm{E}[x_i(t)]_i, \log \mathrm{V}[x_i(t)]_i)$, where M is the number of sample times, yields slope β_s and intercept $\log\alpha_\mathrm{s}$. In either case, R^2 denotes the coefficient of determination for linear fitting.

Our results are based on the coupled oscillator model, where the oscillator i $(i = 1, \ldots, N)$ obeys

*Contact author: mitsui@design.kyushu-u.ac.jp
Present address: Faculty of Design, Kyushu University, Fukuoka, 815-8540 Japan.

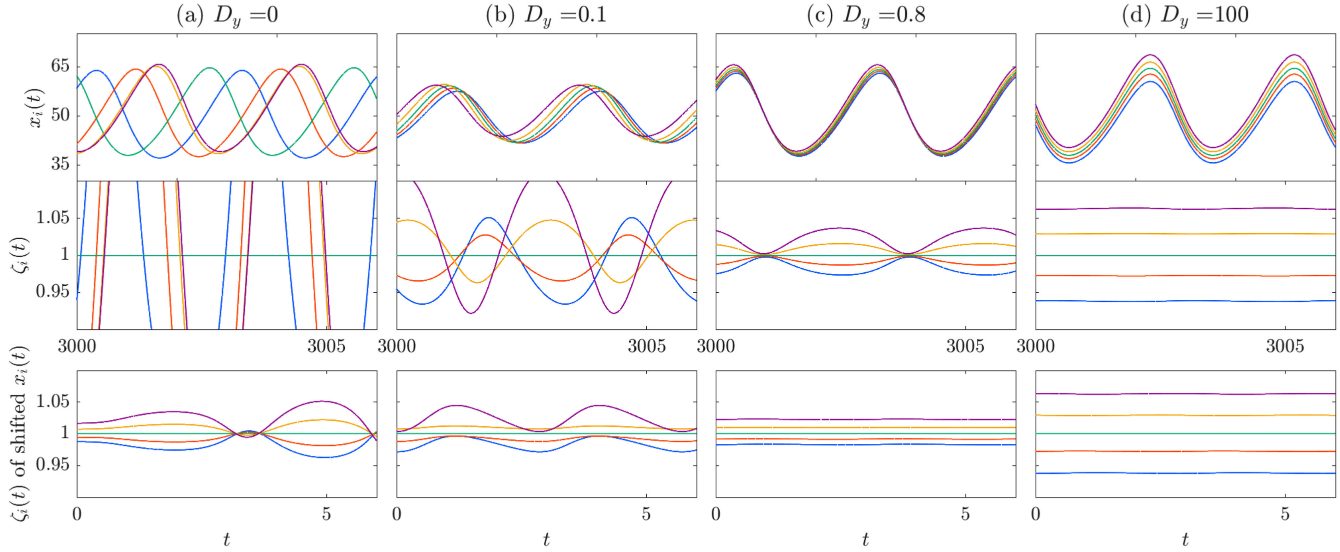

FIG. 1. Examples of $x_i(t)$, $\zeta_i(t)$, and $\zeta_i(t)$ of shifted $x_i(t)$ for each coupling strength. $N = 100, D_x = 0, D_z = 0, a = 1, c = 9, k = 0.6, l = 0.1, x^* = 1.6, y^* = 0$, and $z^* = 0.01$. b_i is randomly selected from a uniform distribution between 4.9 and 5.1. Data for $i = 1, 25, 50, 75$, and 100 are shown. (a) $D_y = 0$, (b) $D_y = 0.1$, (c) $D_y = 0.8$, and (d) $D_y = 100$.

$$\dot{x}_i = f_x(x_i, y_i, z_i) + D_x(X - x_i), \tag{1a}$$

$$\dot{y}_i = f_y(x_i, y_i, z_i) + D_y(Y - y_i), \tag{1b}$$

$$\dot{z}_i = f_z(x_i, y_i, z_i) + D_z(Z - z_i). \tag{1c}$$

We consider a food chain model with global coupling as our first example. Concretely, we consider $f_x = a(x_i - x^*) - lx_iy_i, f_y = -b_i(y_i - y^*) + lx_iy_i - ky_iz_i, f_z = -c(z_i - z^*) + ky_iz_i, X = \langle x_i \rangle_i, Y = \langle y_i \rangle_i$, and $Z = \langle z_i \rangle_i$, where x_i, y_i, and z_i denote the populations of the vegetation, herbivores, and predators at site i, respectively; $\langle w_i \rangle_i = (1/N) \sum_{i=1}^{N} w_i$ is the average of population $w_i\,(w_i = x_i, y_i, z_i)$ over site i; and $a, b_i, c, l, k, x^*, y^*$, and z^* are parameters describing intrinsic dynamical properties [38–40]. The second terms in Eq. (1) describe diffusive coupling with strength D_x, D_y, and D_z. We assume $b_i = b_0 + \mu_i$, where b_0 is the mean $\langle b_i \rangle_i$, and μ_i is the deviation from b_0. Note that $\langle \mu_i \rangle_i = 0$; specifically, μ_i is selected from a uniform distribution between -0.1 and 0.1, and sorted in ascending order. For convenience, we introduced a reference oscillator, $i = 0$, that obeys Eq. (1) with $b_i = b_0$ and $D_x = D_y = D_z = 0$. This model demonstrates synchronized oscillations for a wide range of parameters when the coupling strength is comparable or larger than $\max\{\mu_i\}$. Figure 1 illustrates the typical waveforms of $x_i(t)$. As evident from Figs. 1(b)–1(d), the oscillators are synchronized in frequency under sufficiently strong coupling. Next, we verify temporal and spatial TLs in Fig. 2. TL with $\beta \simeq 2$ is observed when D_y is sufficiently large. Moreover, temporal TL becomes evident for $D_y = 0.8$, whereas spatial TL seems to require stronger coupling. To determine the underlying mechanism of TL, we carefully observed the waveforms shown in Fig. 1(d), which yielded well-defined temporal and spatial TLs. All waveforms were found to be considerably similar.

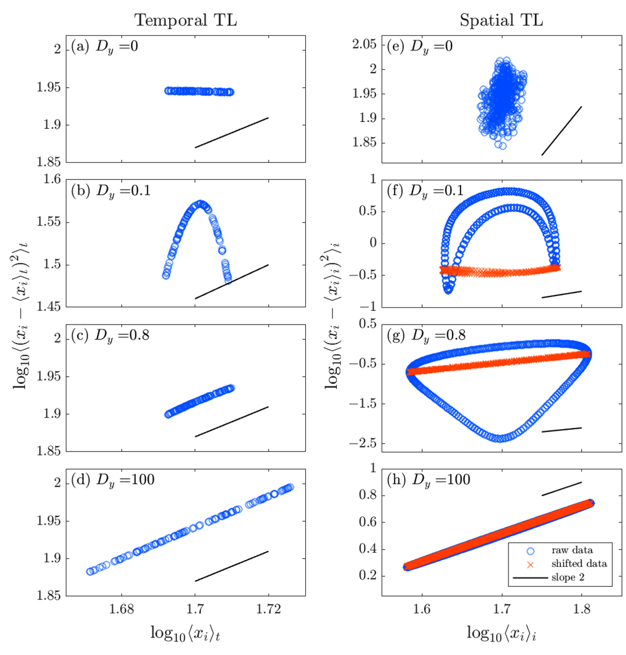

FIG. 2. Examples of TL for each coupling strength. $N = 100, D_x = 0, D_z = 0, a = 1, c = 9, k = 0.6, l = 0.1, x^* = 1.6, y^* = 0$, and $z* = 0.01$. b_i is randomly selected from a uniform distribution between 4.9 and 5.1. Temporal and spatial TLs are shown in the left and right columns, respectively. The blue circles represent the mean-variance relationships of the raw data, red crosses indicate the spatial TL for the shifted data, and black lines are the reference line with a slope 2. Temporal TL for (a) $D_y = 0$, (b) $D_y = 0.1$, (c) $D_y = 0.8$, and (d) $D_y = 100$. Spatial TL for (e) $D_y = 0$, (f) $D_y = 0.1$, (g) $D_y = 0.8$, and (h) $D_y = 100$.

Furthermore, they were approximately proportional to $x_0(t)$ (data not shown). Thus, we hypothesized that the following relation approximately holds true for all i and t: $x_i(t) = C_i x_0(t)$, where C_i is constant; this relation is hereafter referred to as the *waveform proportionality*. With such a relation, both temporal and spatial TLs are evidently valid with $\beta_{\mathrm{t,s}} = 2$, as shown below. First, note that $\mathrm{E}[x_i(t)]_t = C_i \mathrm{E}[x_0(t)]_t$, $\mathrm{V}[x_i(t)]_t = C_i^2 \mathrm{V}[x_0(t)]_t$, $\mathrm{E}[x_i(t)]_i = \mathrm{E}[C_i]_i x_0(t)$, and $\mathrm{V}[x_i(t)]_i = \mathrm{V}[C_i]_i [x_0(t)]^2$. By eliminating C_i and $x_0(t)$ from these relations, we obtain the following temporal and spatial TLs:

$$\mathrm{V}[x_i(t)]_t = \alpha_{\mathrm{t}} \mathrm{E}[x_i(t)]_t^{\beta_{\mathrm{t}}}, \qquad \mathrm{V}[x_i(t)]_i = \alpha_{\mathrm{s}} \mathrm{E}[x_i(t)]_i^{\beta_{\mathrm{s}}}, \quad (2)$$

where

$$\alpha_{\mathrm{t}} = \frac{\mathrm{V}[x_0(t)]_t}{\mathrm{E}[x_0(t)]_t^2}, \qquad \alpha_{\mathrm{s}} = \frac{\mathrm{V}[C_i]_i}{\mathrm{E}[C_i]_i^2}, \quad (3)$$

and $\beta_{\mathrm{t,s}} = 2$. To verify this hypothesis, we plot the ratio $\zeta_i(t) = [x_i(t)/x_j(t)]$, where j is a reference oscillator, as shown in the middle panels of Fig. 1. The choice of j may be arbitrary; here, we selected $j = N/2 = 50$ because $x_{N/2}$ is expected to be close to x_0. Waveform proportionality is visible only in the middle panel of Fig. 1(d), suggesting that waveform proportionality spontaneously emerges in strongly synchronized oscillators, and then, TL with $\beta_{\mathrm{t,s}} = 2$ naturally occurs.

Next, we quantitatively investigate the dependence of the synchronization level and TL parameters on the coupling strength D_y (Fig. 3). We introduce the order parameter χ for synchronization as

$$\chi = \frac{\mathrm{CV}[X(t)]}{\max_i\{\mathrm{CV}[x_i(t)]\}}, \quad (4)$$

where CV represents the coefficient of variation. Namely, χ is the CV of the mean field of $x_i(t)$ normalized by the maximum CV of $x_i(t)$. $\chi \simeq 1$ when the oscillators are strongly synchronized; $\chi \simeq 0$ when the oscillators are desynchronized. Moreover, log $\alpha_{\mathrm{t,s}}$ is illustrated in Fig. S1. Depending on the D_y value, quenching may occur, rendering it impossible to define χ. Thus, we judged that quenching occurred when $(1/N)\sum_{i=1}^N \langle (x_i - \langle x_i \rangle_t)^2 \rangle_t$ was less than a certain threshold value, and such cases were excluded. The number of times we judged quenching occurred is shown in Fig. S2. We confirmed that qualitatively the same results could be obtained for several different threshold values. This process was applied to all systems described later. Simulations were performed up to $t = 3500$, and TL was computed using the time series from $t = 3000$ to $t = 3500$. The error bars represent the standard deviation of ten calculations with different initial conditions and b_i. Unless otherwise noted, initial conditions for numerical simulations were randomly chosen from a uniform distribution between 15 and 15.1.

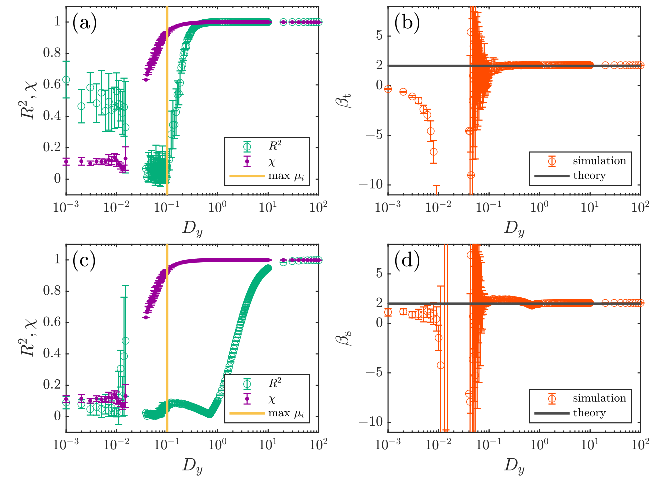

FIG. 3. D_y dependence of TL parameters and synchronization degree of the food chain model. $N = 100, D_x = 0, D_z = 0, a = 1, c = 9, k = 0.6, l = 0.1, x^* = 1.6, y^* = 0,$ and $z^* = 0.01$. b_i is randomly selected from a uniform distribution between 4.9 and 5.1. In (a) and (c), the same χ (purple dot) and $\max\{\mu_i\}$ (orange solid line) are plotted. (a) R^2 of temporal TL. (b) Exponents of temporal TL. (c) R^2 of spatial TL. (d) Exponents of spatial TL.

Figures 3(a) and 3(b) reveal that β_{t} approaches a value close to 2 with large R^2 values as D_y increases. Around $D_y = 0.5$, $R^2 \simeq 1$, and $\beta_{\mathrm{t}} \simeq 2$. Thus, temporal TL with $\beta_{\mathrm{t}} \simeq 2$ was observed around $D_y = 0.5$. In contrast, according to χ, synchronization began at approximately $D_y = 0.05$, significantly earlier than the onset of temporal TL. These results suggest that in addition to synchronization, there exists an unidentified condition responsible for the emergence of temporal TL. Furthermore, the onset of spatial TL was significantly slower than that of temporal TL. To identify the cause of this phenomenon, we focused on the waveform of $D_y = 0.8$, where only temporal TL was observed [Figs. 2(c) and 2(g)]. Here, waveform proportionality was not well realized [Fig. 1(c), middle]; however, when the waveforms were shifted such that their peak positions coincided, the ratio $\zeta_i(t)$ became almost constant, as shown in the bottom panel of Fig. 1(c). This result indicates that the hypothesis $x_i(t) = C_i x_0(t)$ should be replaced with $x_i(t) = C_i x_0(t - t_i)$. t_i is obtained by computing the difference between the time when x_i reaches its local maximum value and the time when x_{50} reaches its local maximum value. Further, the shift t_i was approximately proportional to μ_i and $1/D_y$ as illustrated in Figs. S3 and S4, respectively. These results suggest that waveform proportionality occurs with a lag t_i, which decreases with increasing D_y. Because the first relation of Eq. (2) holds true even when $x_i(t) = C_i x_0(t)$ is replaced with $x_i(t) = C_i x_0(t - t_i)$, temporal TL emerges at small

D_y. In contrast, the second relation of Eq. (2) is violated in the presence of lag; thus, spatial TL may appear only when the lag is vanishingly small, i.e., D_y is considerably large. Accordingly, we found that spatial TL is observed for a wide range of D_y upon using shifted waveforms $x_i(t+t_i)$, as shown in Figs. 2(g) and 2(h) using the red crosses, and Fig. S5.

To theoretically clarify the mechanism underlying the emergence of TL, we performed a perturbative analysis. Motivated by our numerical results, we considered the following ansatzes:

$$x_i(t) = x_0(t-\varepsilon_i\tau) + \varepsilon_i p(t-\varepsilon_i\tau) + O(\hat{\varepsilon}^2), \tag{5a}$$

$$y_i(t) = y_0(t-\varepsilon_i\tau) + \varepsilon_i q(t-\varepsilon_i\tau) + O(\hat{\varepsilon}^2), \tag{5b}$$

$$z_i(t) = z_0(t-\varepsilon_i\tau) + \varepsilon_i r(t-\varepsilon_i\tau) + O(\hat{\varepsilon}^2), \tag{5c}$$

where $\varepsilon_i = \mu_i/D_y$ denotes a nondimensional small parameter; τ is a constant; $p(t)$, $q(t)$, and $r(t)$ are functions to be determined; and $\hat{\varepsilon}$ represents the typical magnitude of the small parameter ε_i. We recall that $x_0(t)$ is a periodic function obeying the following relation for the food chain model under consideration:

$$\dot{x}_0 = f_x(x_0, y_0, z_0) = (a - ly_0)x_0 - ax^*. \tag{6}$$

In Eq. (5), waveform proportionality emerges in $x_i(t)$ if $p(t) \propto x_0(t)$ is approximately true. As shown below, this is true under some conditions. Substituting Eq. (5) into Eq. (1) and extracting the $O(\varepsilon_i)$ terms, we obtain

$$\dot{p} = (a - ly_0 - D_x)p + g(t), \tag{7}$$

where $g(t) = (aD_x\tau - lD_x\tau y_0 - lq)x_0 - aD_x\tau x^*$. Note that Eqs. (6) and (7) are linear in terms of x_0 and p, respectively. Therefore, by assuming that other time-dependent functions are provided, we can solve these equations to obtain the expressions for x_0 and p. As shown in Supplemental Material [41], we obtain

$$x_0(t) = \frac{ax^*}{\bar{f}}\left[A + O\left(\frac{\bar{f}}{\omega}\right)\right]e^{\delta F(t)}, \tag{8a}$$

$$p(t) = -\frac{1}{\bar{f} - D_x}\left[B + O\left(\frac{\bar{f} - D_x}{\omega}\right)\right]e^{\delta F(t)}, \tag{8b}$$

where $\bar{f} = \langle a - ly_0(t)\rangle_t$, $\delta F(t) = \int_0^t [f(t') - \bar{f}]dt'$, $A = \langle e^{-\delta F(t)}\rangle_t$, $B = \langle g(t)e^{-\delta F(t)}\rangle_t$. Therefore, $p(t)$ becomes approximately proportional to $x_0(t)$ when the following conditions are satisfied:

$$A \gg O\left(\frac{\bar{f}}{\omega}\right), \qquad B \gg O\left(\frac{\bar{f} - D_x}{\omega}\right). \tag{9}$$

Thus, TL with exponent $\beta_{\mathrm{t,s}} = 2$ should be observed in good approximation when ε_i is sufficiently small. Furthermore, substituting Eqs. (8a) and (8b) into Eq. (2), and omitting the $O(\cdot)$ terms, we obtain

$$\alpha_{\mathrm{t}} = \frac{\mathrm{V}[e^{\delta F}]_t}{\mathrm{E}[e^{\delta F}]_t^2}, \qquad \alpha_{\mathrm{s}} = \left(\frac{\bar{f}}{\bar{f} - D_x}\frac{B}{ax^*A}\right)^2 \mathrm{V}[\varepsilon_i]_i. \tag{10}$$

We expect that Eq. (9) can be generally satisfied when $\bar{f}$ and D_x are sufficiently smaller than ω. In the present example, $\omega \simeq 2.18$, $\bar{f} \simeq 0.0327$, and $D_x = 0$, which confirm the validity of our approximation. Indeed, the predicted $\beta_{\mathrm{t,s}}$ and $\log \alpha_{\mathrm{t,s}}$, shown using the black lines and dots in Fig. 3 and Fig. S1, are in excellent agreement with the simulation results for large D_y. One might naively expect that waveform proportionality naturally arises for oscillators with strong diffusive coupling because the waveforms become virtually identical in the strong coupling limit. However, note that convergence $[p(t) \to 0]$ does not imply waveform proportionality, and the manner of convergence is crucial. An interesting prediction, possibly opposing the naive expectation, is that waveform proportionality is violated when D_x is large because a large D_x will violate Eq. (9). We numerically demonstrate this prediction in Fig. S6 by considering the $D_x > 0$ case. In contrast, there is no condition corresponding to D_z. Indeed, as shown in Fig. S7, TL is observed for $D_z > 0$.

Next, we generalize our theory considering the following situation. Suppose we have N oscillators, each of which can be described by an M-dimensional dynamical system. Let $x_i(t)\,(i = 1, \ldots, N)$ be the observables obeying $\dot{x}_i = s_i(t)x_i + u_i(t)$, where $s_i(t)$ and $u_i(t)$ are periodic with period $(2\pi/\omega)$. Assume $s_i(t) = s(t) + \varepsilon_i\delta s(t)$ and $u_i(t) = u(t) + \varepsilon_i\delta u(t)$ to the lowest order in ε_i, where $s, u, \delta s$, and δu are periodic. Then, the above analysis can similarly be applied to this system. Accordingly, we conclude that waveform proportionality occurs in $x_i(t)$ for small ε_i if Eq. (9), wherein $\bar{f}$ is replaced with $\langle s(t)\rangle_t$, is satisfied. Essentially, the equation should be linear in terms of observables and its intrinsic dynamics should be sufficiently slow. When these assumptions are satisfied, the approximation is effective, resulting in waveform proportionality. Furthermore, we note that our theory can approximately be extended to a class of chaotic oscillators. Suppose that $s_i(t)$ and $u_i(t)$ show chaotic oscillations with characteristic period T. We assume that the time averages of $s_i(t)$ and $u_i(t)$ over 1 period T do not strongly fluctuate from the long-time averages of $s_i(t)$ and $u_i(t)$. Under this assumption, the above arguments hold approximately true. Based on these observations, we predict that TL can arise in a broad class of systems, including various types of (i) chaotic oscillators, (ii) coupling mechanisms, and (iii) dynamical systems. For (i) chaotic oscillators, we demonstrate that the same food chain model with another set of parameters that yields chaotic oscillations approximately shows waveform proportionality and TL when the oscillators are synchronized (Fig. S8). For (ii) coupling mechanisms, we demonstrate that TL is observed in a pacemaker-driven system, with $Y = y_0$ in Eq. (1) (Fig. S9). For (iii) dynamical systems, as an example, we consider the following Rössler system [40,42–46]: $f_x = -(\omega_0 + \mu_i)y_i - z_i, f_y = (\omega_0 + \mu_i)x_i + ay_i$, and $f_z = b + z_i(x_i - c)$ in Eq. (1). Note that the actual frequency, ω, is approximately equal to ω_0 in this system. We consider $D_x = D_y = D > 0$ and $D_z = 0$. The results of this system are shown in Fig. S10. Here, we use parameters $a = 0.1$, $b = 0.1$, and $c = 0.7$, which indicate periodic oscillations because the typical parameters $a = 0.2$, $b = 0.2$, and $c = 5.7$, which indicate chaotic behavior, violate condition Eq. (9). In this system, TL is expected to be observed in variable z_i when Eq. (9) is satisfied wherein D_x and $\bar{f}$ are replaced with 0 and $\langle x_0(t) - c\rangle_t$, respectively. Furthermore, we investigate ω_0 dependency with fixed D because the validity of Eq. (9) can conveniently be controlled through ω_0. As expected, $\beta_{\mathrm{t,s}}$ approaches 2 with large R^2 values as ω_0 increases (Fig. S11). Further, we analytically and numerically confirm the waveform proportionality and TL with an exponent 2 in the coupled Lorenz system [47] and coupled Brusselator [48], shown in Figs. S12 and S13, respectively. Although our theory presented in this Letter cannot be applied to the coupled Lorenz system, we have been able to perform analytical calculations by constructing another theory [49].

Discussion—In this study, we showed that temporal and spatial TLs are induced by synchronization in a broad class of periodic and chaotic oscillators. Specifically, we demonstrated that as the degree of synchronization increases, the correlation between log (mean) and log (variance) becomes stronger. Moreover, we showed that in regions of strong synchronization, waveform proportionality emerges, resulting in the derivation of temporal and spatial TLs with $\beta = 2$. In these synchronization-induced TLs, temporal and spatial TLs arise in the same mechanism, i.e., waveform proportionality. In contrast, owing to phase lag, which is expressed by the $\varepsilon_i\tau$ terms in Eq. (5), spatial TL requires stronger coupling than temporal TL. While several studies explored the relationship between TL and synchronization [20,21,24–27,30,37,50], most of them investigated the correlation between the exponents of TL and the degree of synchronization through numerical simulations. Reuman *et al.* derived the analytical relationship between spatial TL and synchronization [24]. In this study, we analytically derived both temporal and spatial TLs with $\beta = 2$ from the synchronization state. Although other mechanisms are known to exist for TL with $\beta = 2$ [3,17,19,23,29,31–35], we believe that our findings provide valuable insights into the understanding of TL from the perspective of synchronization as another universal phenomenon in ecosystems [51]. Our results can help in inferring the existence of synchronization solely from the relationship between mean and variance [52]. This research also suggests that coupling strength may be inferred by quantifying the similarity of waveforms.

Parameter heterogeneity plays an essential role in this study. For example, the range of temporal TL plots in Fig. 2 widens with parameter heterogeneity. However, for some systems, increasing the heterogeneity may lead to divergence or loss of synchronized oscillation, in which case TL is lost; the range of the parameter heterogeneity that causes TL is limited by the range over which synchronized oscillation occurs.

Phenomena similar to waveform proportionality, including the projective synchronization [53] and a type of generalized synchronization [54] have been previously proposed. These previously reported phenomena are observed in a limited class of coupled oscillators. We showed that waveform proportionality emerges in a broad class of strongly synchronized coupled periodic and chaotic oscillators. It is important to understand the behavior of strongly coupled systems because there are various systems that require strong coupling to ensure stability, such as the heart [55], power grids [56], and next-generation communications using chaotic synchronization [57]. In this context, we clarified general properties that appear in strongly coupled periodic and chaotic oscillators, namely, waveform proportionality and TL with an exponent 2 resulting from it.

Acknowledgments—This study was supported by JSPS KAKENHI Grant No. 23KJ0830 and WINGS CFS program of The University of Tokyo to Y. M., and JSPS KAKENHI Grant No. 21K12056 to H. K.

[1] C. I. Bliss, J. Econ. Entomol. **34**, 221 (1941).
[2] L. R. Taylor, Nature (London) **189**, 732 (1961).
[3] A. S. Sassi, M. Garcia-Alcala, M. Aldana, and Y. Tu, Phys. Rev. X **12**, 011051 (2022).
[4] M. A. de Menezes and A. L. Barabási, Phys. Rev. Lett. **92**, 028701 (2004).
[5] M. A. de Menezes and A. L. Barabási, Phys. Rev. Lett. **93**, 068701 (2004).
[6] J. Duch and A. Arenas, Phys. Rev. Lett. **96**, 218702 (2006).
[7] Z. Eisler, I. Bartos, and J. Kertész, Adv. Phys. **57**, 89 (2008).
[8] R. A. J. Taylor, *Taylor's Power Law: Order and Pattern in Nature*, 1st ed. (Academic Press, New York, 2019).
[9] V. Narayan, S. Ramaswamy, and N. Menon, Science **317**, 105 (2007).
[10] J. Deseigne, O. Dauchot, and H. Chaté, Phys. Rev. Lett. **105**, 098001 (2010).
[11] F. Ginelli, F. Peruani, M. Bär, and H. Chaté, Phys. Rev. Lett. **104**, 184502 (2010).
[12] S. Ngo, A. Peshkov, I. S. Aranson, E. Bertin, F. Ginelli, and H. Chaté, Phys. Rev. Lett. **113**, 038302 (2014).
[13] B. Mahault, F. Ginelli, and H. Chaté, Phys. Rev. Lett. **123**, 218001 (2019).

[14] F. Ginelli, Eur. Phys. J. Special Topics **225**, 2099 (2016).
[15] H. Chaté, Annu. Rev. Condens. Matter Phys. **11**, 189 (2020).
[16] D. Nishiguchi, J. Phys. Soc. Jpn. **92**, 121007 (2023).
[17] J. E. Cohen, Theor. Ecol. **7**, 77 (2014).
[18] J. E. Cohen, Theor. Popul. Biol. **93**, 30 (2014).
[19] J. E. Cohen, M. Xu, and W. S. Schuster, Proc. R. Soc. B **280** (2013).
[20] A. J. Kerkhoff and F. Ballantyne IV, Ecol. Lett. **6**, 850 (2003).
[21] L. Zhao, L. W. Sheppard, P. C. Reid, J. A. Walter, and D. C. Reuman, J. Anim. Ecol. **88**, 484 (2019).
[22] J. E. Cohen and M. Xu, Proc. Natl. Acad. Sci. U.S.A. **112**, 7749 (2015).
[23] A. Giometto, M. Formentin, A. Rinaldo, J. E. Cohen, and A. Maritan, Proc. Natl. Acad. Sci. U.S.A. **112**, 7755 (2015).
[24] D. C. Reuman, L. Zhaoa, L. W. Sheppard, P. C. Reid, and J. E. Cohen, Proc. Natl. Acad. Sci. U.S.A. **114**, 6788 (2017).
[25] J. E. Cohen and T. Saitoh, Ecology **97**, 3402 (2016).
[26] T. Saitoh, Popul. Ecol. **62**, 300 (2020).
[27] F. Ballantyne IV and A. J. Kerkhoff, J. Theor. Biol. **235**, 373 (2005).
[28] J. N. Perry, Proc. R. Soc. B **257**, 221 (1994).
[29] F. Ballantyne IV, Evol. Ecol. Res. **7**, 1213 (2005), https://www.evolutionary-ecology.com/abstracts/v07/1876.html.
[30] F. Ballantyne IV and A. J. Kerkhoff, Oikos **116**, 174 (2007).
[31] J. E. Cohen, Theor. Popul. Biol. **88**, 94 (2013).
[32] R. M. Anderson, D. M. Gordon, M. J. Crawley, and M. P. Hassel, Nature (London) **296**, 245 (1982).
[33] A. M. Kilpatrick and A. R. Ives, Nature (London) **422**, 65 (2003).
[34] S. Carpenter, S. Callens, C. Brown, J. E. Cohen, and B. Z. Webb, Theor. Popul. Biol. **154**, 118 (2023).
[35] M. Salahshour, New J. Phys. **25**, 123012 (2023).
[36] L. R. Taylor and I. P. Woiwod, J. Anim. Ecol. **51**, 879 (1982).
[37] I. Hanski, Oikos **50**, 148 (1987).
[38] B. Blasius, A. Huppert, and L. Stone, Nature (London) **399**, 354 (1999).
[39] B. Blasius and L. Stone, Int. J. Bifurcation Chaos **10**, 2361 (2000).
[40] E. Montbrió and B. Blasius, Chaos **13**, 291 (2003).
[41] See Supplemental Material at http://link.aps.org/supplemental/10.1103/PhysRevLett.134.167202 for calculation details and additional simulation results.
[42] M. G. Rosenblum, A. S. Pikovsky, and J. Kurths, Phys. Rev. Lett. **76**, 1804 (1996).
[43] M. G. Rosenblum, A. S. Pikovsky, and J. Kurths, Phys. Rev. Lett. **78**, 4193 (1997).
[44] H. Sakaguchi, Phys. Rev. E **61**, 7212 (2000).
[45] A. S. Pikovsky, M. G. Rosenblum, and J. Kurths, Europhys. Lett. **34**, 165 (1996).
[46] G. V. Osipov, A. S. Pikovsky, M. G. Rosenblum, and J. R. Kurths, Phys. Rev. E **55**, 2353 (1997).
[47] K. J. Lee, Y. Kwak, and T. K. Lim, Phys. Rev. Lett. **81**, 321 (1998).
[48] H. Daido, Phys. Rev. E **84**, 016215 (2011).
[49] We can show waveform proportionality and TL with an exponent 2 not only for the Lorenz system, but also for generalized Lorenz systems. A paper on these results is in preparation.
[50] I. Hanski and I. P. Woiwod, J. Anim. Ecol. **62**, 656 (1993).
[51] A. Liebhold, W. D. Koenig, and O. N. Bjørnstad, Annu. Rev. Ecol. Evol. Syst. **35**, 467 (2004).
[52] G. Petri, P. Expert, H. J. Jensen, and J. W. Polak, Sci. Rep. **3**, 1798 (2013).
[53] R. Mainieri and J. Rehacek, Phys. Rev. Lett. **82**, 3042 (1999).
[54] T. Kano and K. Umeno, Chaos **32**, 113137 (2022).
[55] J. Keener and J. Sneyd, *Mathematical Physiology*, 2nd ed. (Springer, New York, 2009).
[56] P. J. Menck, J. Heitzig, J. Kurths, and H. J. Schellnhuber, Nat. Commun. **5**, 3969 (2014).
[57] D. Moreno, S. Fujii, A. Nakashima, D. Lemcke, A. Uchida, P. Sanchis, and T. Tanabe, Opt. Express **32**, 2460 (2024).